博士論文　（要約）

Structural analysis of the extracellular domain of PTPδ
(PTPδ の細胞外ドメインの構造解析)

Li Yanjun

李　彦君

Contents

Abstract

Mammalian brains are composed of a few hundred billions of neurons. These large quantities of neurons are connected by synapses to establish and maintain higher-order brain functions. Synapses are specialized cell adhesions which enable cell-cell communications between neurons. Synapse formation in the central nervous system (CNS) requires the collaboration of various molecules to ensure synapse specificity. One crucial molecular family which is involved in the recognition of target cells as well as the formation and maintenance of the synapses is the cell-adhesion molecules (CAMs). Type IIa receptor protein tyrosine phosphatases (RPTPs), also known as LAR subfamily of RPTPs, are among the most-characterized synaptic CAMs.

Type IIa RPTPs are originally linked to axon guidance and are recently highlighted as synaptic organizers which induce synaptic differentiation as well as synaptic organization during neural development. The family of type IIa RPTPs in vertebrates is composed of three members: LAR, PTPσ, and PTPδ. Each vertebrate member in type IIa RPTP subfamily contains an intracellular domain, a single transmembrane helix and a large extracellular domain (ECD). Presynaptic type IIa RPTP proteins interact with various postsynaptic adhesion molecules and form transsynaptic adhesion complexes to regulate both excitatory and inhibitory synapse development.

Although the structural mechanism of the interaction between type IIa RPTPs and their postsynaptic ligands has been extensively studied by crystallography and other biophysical techniques, it remains unclear how the extracellular interaction transmits the signal into the intracellular domain, partly due to the lack of the structural information of the extracellular juxtamembrane region (EJR) of type IIa RPTPs.

In this study, the crystal structure of mouse PTPδ FN3-EJR and zebrafish PTPδ FN3-

EJR have been revealed. This study provides the first atomic details of the EJR domain in type IIa RPTPs and provides the structural basis for the further functional study of this important extracellular juxtamembrane region.

Chapter 1
Introduction

1.1 Synapse formation and cell adhesion molecules

Mammalian brains are composed of a few hundred billions of neurons. These large quantities of neurons are connected by synapses to establish and maintain higher-order brain functions such as emotion, learning and memory [1]. To understand how neurons execute sensory-motor functions and produce thoughts or actions, we have to investigate the basic structure of neuron-neuron network—the synapse (Figure 1-1) [2]. Synapses are specialized cell adhesions which enable cell-cell communications between neurons. The neurotransmitters are released into the synaptic cleft and they diffuse across the cleft to recognize and interact with their corresponding postsynaptic receptors. Then the neurotransmitters activate their receptors to transmit signals [2].

The processes of searching, recognizing, and binding to specific synaptic partner is very complicated. Thus, synapse formation in the central nervous system (CNS) requires the collaboration of various molecules to ensure synapse specificity [3]. One crucial molecular family which is involved in the recognition of target cells as well as the formation and maintenance of the synapses is the cell-adhesion molecules (CAMs) (Figure 1-2) [4]. CAMs are proteins located on the cell surface and they promote the specific cells to stick to each other. Since CAMs are in charge of joining adjacent cells, they are able to promote the formation of synapses between two neurons through a variety of processes. Previous studies have elucidated that during the early phase of synapse development, CAMs play a role in cell migration, synapse plasticity, and axon guidance. However, they switch tasks and take part in maintaining synaptic stability instead during the later phase [2]. CAMs usually contain three conserved domains: a large extracellular domain, a simple transmembrane domain and a relatively small intracellular domain. In synapse formation, the extracellular domain may be the most significant part since it is

supposed to be involved in synaptogenesis via the regulation of docking geometries [2].

1.2 Type IIa receptor protein tyrosine phosphatases

Type IIa receptor protein tyrosine phosphatases (RPTPs), also known as LAR subfamily of RPTPs, are among the most-characterized synaptic CAMs [4-6]. Type IIa RPTP family includes one worm member (PTP-3), two fly members (DPTP69D and Dlar) and three vertebrate members (LAR, PTPσ and PTPδ) [6]. Type IIa RPTPs are specifically expressed in the central nervous systems of vertebrates, leech and Drosophila during axon guidance and synapse formation [7-10]. Type IIa RPTPs are originally linked to axon guidance and are recently highlighted as synaptic organizers which induce synaptic differentiation as well as synaptic organization during neural development [11].

Each vertebrate member in type IIa RPTP subfamily contains an intracellular domain, a single transmembrane helix and a large extracellular domain (ECD) (Figure 1-3). The intracellular domain consists of two protein tyrosine phosphatase domains D1 and D2. The membrane-proximal domain D1 has catalytic activity, whereas the membrane-distal domain D2 is inactive. The ECD consists of three immunoglobulin-like (Ig) domains and four or eight fibronectin type-III (FN) domains [12]. The length and function of the ECD are regulated by alternative splicing. Recent studies indicated that alternative splicing in MeA or MeB sites in Ig domains can control the ligand-binding specificity of type IIa RPTPs [13-15].

Presynaptic type IIa RPTP proteins interact with various postsynaptic adhesion molecules (Figure 1-4) and form transsynaptic adhesion complexes to regulate both excitatory and inhibitory synapse development [16]. Individual family members may participate in the assembly of specific synapse types. LAR and PTPσ take part in

excitatory synapse formation, whereas PTPδ play a role in both excitatory and inhibitory synapse formation [17]. A proper balance of excitation and inhibition in synapses is important for normal information transmission in CNS and pathological changes in this balance may cause brain disorders such as autism spectrum disorder [18] and bipolar disorder [19].

1.3 Juxtamembrane domain

Transmembrane receptors take part in various biological processes [20]. For those receptors which contain a single transmembrane (TM) helix, like cell adhesion receptors, receptor tyrosine kinases and immune receptors, major attentions have been paid on their extracellular ligand-binding domains. However, during the past decades, it has been discovered that the TM helix in these proteins may play an active role in signal transmission. The movement of the TM helix is limited, usually within several angstroms during signal transmission. Thus, it becomes a topic of interest that how this slight movement can cause a great change in post-translational modification of the receptor and in the processes of association and dissociation with its downstream binding partners. Some recent studies indicated that the juxtamembrane (JM) region near the TM helix also plays a direct role in the process of signal transmission.

It is suggested that the rotation of the extracellular part of growth hormone receptor (GHR) TM helical dimer can be induced by the binding of growth hormone and then triggers a separation of the intracellular part of the TM helical dimer. In other words, the conserved JM regions on both extracellular and intracellular sides of the TM helix modulate the activation of GHR [21]. Similarly, eltrombopag binds to the extracellular JM region and TM helix of thrombopoietin receptor (TpoR) to modulate the activation of

TpoR thus stimulate megakaryopoiesis and platelet production [22-24]. Tropomyosin receptor kinase (Trk) receptors are tyrosine kinase receptors which can trigger the signal transduction cascade. Trk protein consists of an intracellular kinase domain, a single TM region and an extracellular domain [25]. Recent studies indicated that the extracellular juxtamembrane region (EJR) of TrkB is involved in the inhibition of TrkB dimerization. Molecular perturbation on the EJM can induce some conformational changes, leading to the activation of TrkB [26]. Moreover, many adhesion receptors transmit signals across the plasma membrane upon ligand binding. In some cases, the JM region appears to regulate the self-association of the adhesion receptor or the association with other proteins [27, 28].

1.4 Objective

Although the structural mechanism of the interaction between type IIa RPTPs and their postsynaptic ligands has been extensively studied by crystallography and other biophysical techniques, it remains unclear how the extracellular interaction transmits the signal into the intracellular domain, partly due to the lack of the structural information of the extracellular juxtamembrane region (EJR) of type IIa RPTPs.

Even though the function of EJR domain of type IIa RPTPs remains unclear, some general functions of juxtamembrane domains in various proteins have been elucidated so far. The juxtamembrane region in diverse proteins may have various functions: make the neural signal more substantial or more recognizable, modulate the activation of the host receptor, modulates the outside-in signaling of adhesion receptors, help to maintain the inactive conformation of the kinase domain, undergo a conformational change during dimerization, inhibit protein dimer formation thus regulate protein activation, as well as

keep the overall structural stability of the protein.

Furthermore, type IIa RPTPs are expressed on the cell surface and processed by furin protease to obtain two subunits derived from a proprotein [29, 30]. It was suggested that these two subunits can still associated non-covalently even after the furin cleavage and the binding of them is sufficiently strong to resist kinds of disruption [29]. It was also demonstrated that one subunit contains the Ig domains and FN domains, whereas the other subunit contains a small part of the extracellular domain, the transmembrane region and the intracellular domains. As the proteolytic processing is essential for the biological function of type IIa RPTPs, it is important to shed a light on the binding mechanism of these two associated subunits. A crucial step is to reveal the structure basis of type IIa RPTP extracellular region that contains furin cleavage site, which is the EJR domain in this study.

In this study, I isolated a region including the EJR from mouse or zebrafish PTPδ, and investigated the structural feature of the extracellular domain of PTPδ near the cell membrane. This study provides the first atomic details of the EJR domain in type IIa RPTPs and provides the structural basis for the further functional study of this important extracellular juxtamembrane region.

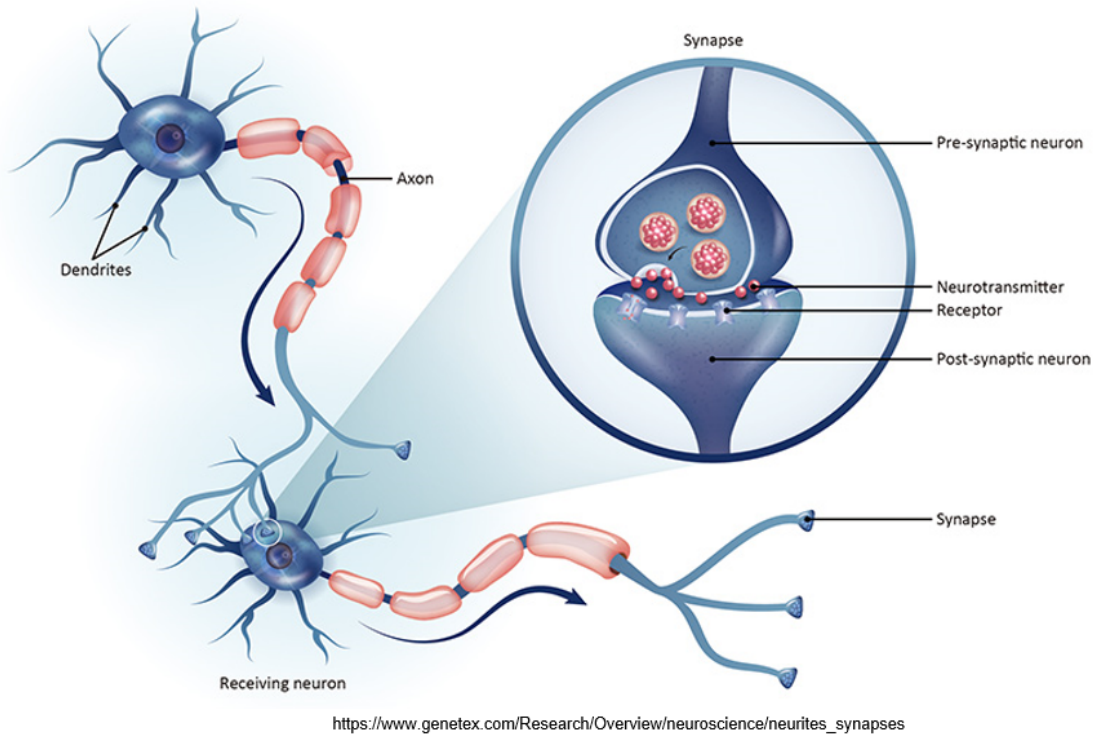

Figure 1-1 Neuron-neuron network and the synapse.

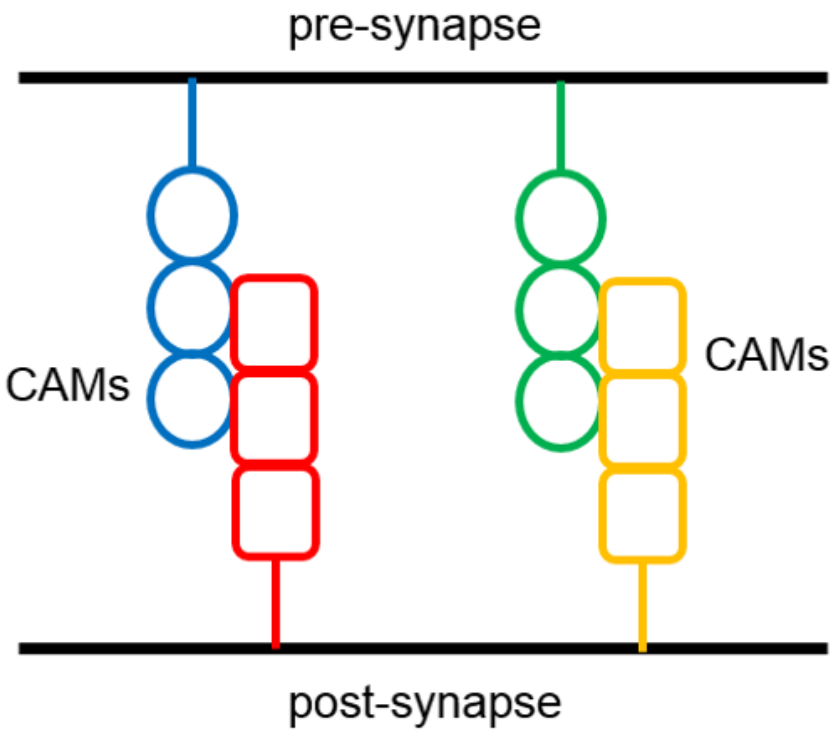

Figure 1-2 Schematic diagram of CAMs participated in synapse formation. Extracellular domains of different kinds of CAMs are colored blue, red, green and yellow.

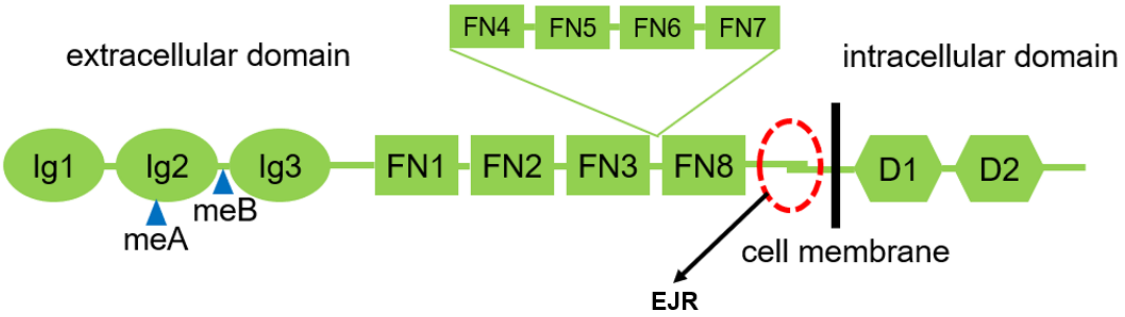

Figure 1-3 Domain organization of type IIa RPTPs. The intracellular domain consists of two protein tyrosine phosphatase domains D1 and D2. The extracellular domain consists of three Ig domains and four or eight FN domains. Alternative splicing sites meA and meB are indicated by blue arrows.

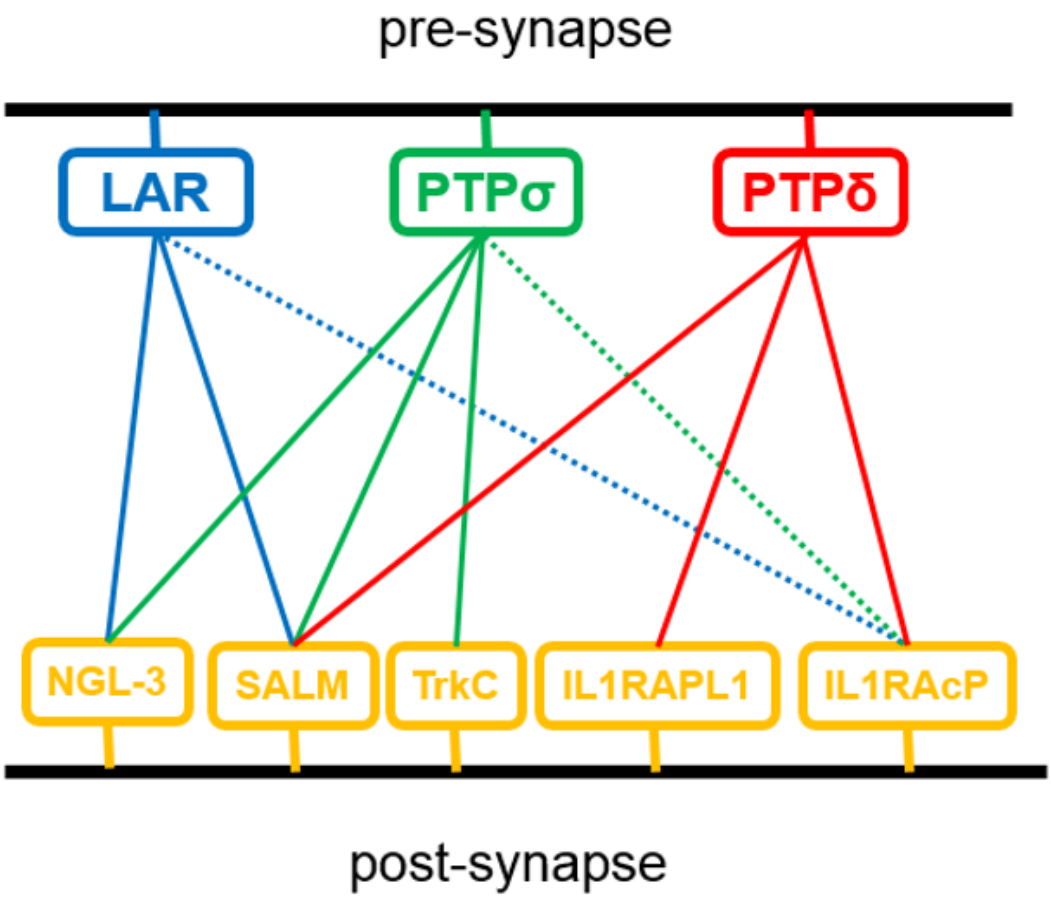

Figure 1-4 Type IIa RPTPs and some of their postsynaptic binding partners. Preferential binding pairs between Type IIa RPTPs and postsynaptic ligands are indicated by solid lines, and relatively weak interactions are indicated by dotted lines.

Chapter 2
Protein expression and purification of mouse PTPδ FN3-EJR

2.1 Introduction

Selenium has an X-ray absorption edge at 0.98 Å and can be introduced into proteins by the substitution of selenomethionine for methionine. Selenomethionine (SeMet)-labeled proteins and their native proteins usually differ only very slightly, or have no difference at all [31]. SeMet is extensively used in protein crystallization for multi- or single- wavelength anomalous diffraction (MAD or SAD). The anomalous signals of SeMet molecules can be used for phasing and for subsequent model building [32]. B834(DE3) is a kind of methionine auxotroph and allows high specific-activity labeling of target proteins with selenomethionine for crystallography [33].

In this chapter, I constructed the protein expression system of SeMet-labeled mouse PTPδ FN3-EJR, using pET28aSUMO plasmid and *E.coli* strain. After the expression check, SeMet-labeled protein was expressed in large-scale SeMet medium and purified with affinity chromatography, anion exchange chromatography and size exclusion chromatography. Finally, the highly purified SeMet-labeled mouse PTPδ FN3-EJR was concentrated for crystallization.

2.2 Materials and Methods

2.2.1 Expression system construction of mouse PTPδ FN3-EJR

The gene encoding mouse PTPδ FN3-EJR was amplified by PCR with KOD-Plus-Neo polymerase (TOYOBO). The reaction solution components and cycling conditions are described in Figure 2-1.

The plasmid pET28aSUMO with N-terminal hexa-histidine (His_6)-SUMO tag was kindly provided by Dr. Sato, and digested with the restriction enzyme NdeI (New England Biolabs) at 37°C for 2 h.

The DNA of mouse PTPδ FN3-EJR was assembled with linearized pET28aSUMO by Gibson Assembly.

The verified recombinant plasmids were transformed into *E. coli* cells by electroporation.

2.2.2 Expression check of mouse PTPδ FN3-EJR

Freshly transformed colonies were inoculated into 5 mL LB medium containing kanamycin and incubated at 37°C overnight. 200 μL *E.coli* suspension was transferred into 5 mL LB medium containing kanamycin and another 200 μL *E.coli* suspension was transferred into 5 mL SeMet medium containing kanamycin. These solutions were incubated at 37°C until OD_{600} reached 0.6. Protein expressions were induced by adding isopropyl-β-D-1-thiogalactopyranoside (IPTG). After incubation overnight, the cells were harvested by centrifugation at 5000 rpm for 10 min and resuspended in 1 mL lysis buffer. Resuspended cells were lysed by sonication and centrifugated at 15000 rpm for 10 min at 4°C to remove cell debris. The supernatant was then applied to Ni-NTA Superflow resin (Qiagen) pre-equilibrated with lysis buffer and incubated at 4°C for 15 min. The

supernatant fraction was removed after centrifugation at 700 × g for 5 min, then 200 μL lysis buffer was added to Ni-NTA resin for washing. After centrifugation at 700 × g for 5 min, the supernatant fraction was removed and the resin was sampled for SDS-PAGE analysis.

2.2.3 Large-scale expression and purification of mouse PTPδ FN3-EJR

E.coli colonies were inoculated into 30 mL LB medium containing kanamycin and incubated at 37°C overnight. The 30 mL *E.coli* suspension was transferred into 2.5 L SeMet medium containing kanamycin and incubated at 37°C until OD_{600} reached almost 0.6. IPTG was added to induce protein expression. After incubation overnight, the cells were harvested by centrifugation at 7000 rpm for 10 min and resuspended in 100 mL lysis buffer. Resuspended cells were lysed by sonication and centrifugated at 17000 rpm for 1h at 4°C.

The supernatant was applied to Ni-NTA Superflow resin pre-equilibrated with lysis buffer and incubated at 4°C for 15 min. The fraction of flow through was collected for sampling and the Ni-NTA column was washed with 50 mL wash buffer. Protein was eluted with 25 mL elution buffer. Ubiquitin-like-specific protease 1 (ULP1) was added to the protein elution with the ratio of 1:200 (w/w) to cleave down the His_6-SUMO tag. The elution was dialyzed against dialysis buffer at 4°C overnight to lower the concentration of NaCl.

Anion exchange chromatography was applied for protein purification with Resource Q 6 mL column (GE Healthcare). The buffers were filtered and degassed, then stored at 4°C for use. The protein fractions were collected and concentrated to 500 μL with Vivaspin 20 (10000 MWCO PES) (Sartorius). The sample was then applied to a HiLoad

16/60 Superdex 75 column (GE Healthcare) for size exclusion chromatography. Protein purification processes were performed by AKTApurifier (GE Healthcare). The purified fractions were confirmed by SDS-PAGE and concentrated to approximately 10 g/L with Vivaspin 20 (10000 MWCO PES) (Sartorius). The absorbance of the protein at 280 nm was measured with Nanodrop ND2000 (Thermo Fisher), and the concentration of the protein was calculated by the absorbance at 280 nm and the molar extinction coefficient. The concentrated protein sample was dispensed into several microtubes, flash frozen in liquid nitrogen and stored at -80°C.

2.3 Results and Discussion

2.3.1 Expression check of mouse PTPδ FN3-EJR

The recombinant mouse PTPδ FN3-EJR was expressed in *E. coli* cells and can be found in the soluble fraction after lysis (Figure 2-2). The band of His_6-SUMO-PTPδ can be detected in resin fraction on SDS-PAGE gel, indicates that his_6-SUMO-PTPδ bond to Ni-NTA resin successfully by the binding affinity of His_6 toward Ni-NTA. By comparing the approximate protein expression level in LB medium and in SeMet medium, I found that there was no distinct difference between the protein yields of these two kinds of medium. This indicated that it is possible to obtain abundant SeMet-labeled mouse PTPδ FN3-EJR by using SeMet medium. Large-scale expression in 2.5 L SeMet medium was performed after the expression check.

2.3.2 Large-scale expression and purification of mouse PTPδ FN3-EJR

The supernatant containing His_6-SUMO-tagged mouse PTPδ FN3-EJR was added to Ni-NTA resin for affinity chromatography, and the result is shown in Figure 2-3. The target protein mainly existed in supernatant, while there was still a small amount of target protein existed in precipitate. His_6-SUMO-PTPδ FN3-EJR bond to Ni-NTA resin and most of contaminant proteins were removed after washing. Most of the target protein was then eluted into the fraction of elution while a small amount of the protein remained on the Ni-NTA resin. The concentration of the proteins in elution was calculated to be 4.69 g/L by the absorbance at 280 nm and the molar extinction coefficient of His_6-SUMO-PTPδ FN3-EJR. After the overnight digestion with ULP1, mouse PTPδ FN3-EJR was successfully cleaved away from His_6-SUMO tag.

The protein mixture of mouse PTPδ FN3-EJR and His_6-SUMO was further purified

by anion-exchange chromatography and size exclusion chromatography to remove His_6-SUMO and obtain highly purified mouse PTPδ FN3-EJR. The protein sample was subjected to a Resource Q 6 mL column (GE Healthcare) and mouse PTPδ FN3-EJR was eluted at a NaCl concentration of approximately 0.1 M. The eluted fractions A4-B10 were analyzed by SDS-PAGE (Figure 2-4). Fractions which were rich in our target protein, were concentrated and further purified by a HiLoad 16/60 Superdex 75 column (GE Healthcare). There was only one sharp peak during size exclusion chromatography, but two protein bands appeared on SDS-PAGE gel (Figure 2-5). The target protein and His_6-SUMO should have been separated after size exclusion chromatography because their molecular weights were quite different. Some weak interaction may still exist between mouse PTPδ FN3-EJR and His_6-SUMO even after the protease cleavage. The protein sample was subjected to a Ni-NTA column to almost completely remove the remaining His_6-SUMO tag. The highly purified mouse PTPδ FN3-EJR was concentrated to 2200 μL. The concentration of the protein was calculated to be 10.50 g/L by the absorbance at 280 nm and the molar extinction coefficient of mouse PTPδ FN3-EJR.

2.4 Summary

In this chapter, the expression system of mouse PTPδ FN3-EJR was constructed for protein expression in *E.coli* cells. After confirming the expression level in small scale, SeMet-labeled mouse PTPδ FN3-EJR was expressed in large scale and purified by Ni-NTA affinity chromatography, followed by anion exchange chromatography and size exclusion chromatography. Finally, SeMet-labeled mouse PTPδ FN3-EJR was highly purified and concentrated for crystallization.

Reaction solution:

Milli-Q water	6.8 μL
10× KOD Plus Neo buffer	1 μL
2 mM dNTPs	1 μL
25 mM $MgSO_4$	0.6 μL
10 pmol/μL forward primer	0.2 μL
10 pmol/μL reverse primer	0.2 μL
template DNA	0.05 μL
KOD Plus Neo	0.2 μL
Total reaction volume	10 μL

PCR cycling conditions:

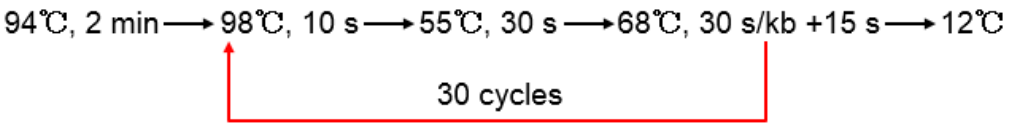

Figure 2-1 PCR reaction solution components and cycling conditions of mouse PTPδ FN3-EJR.

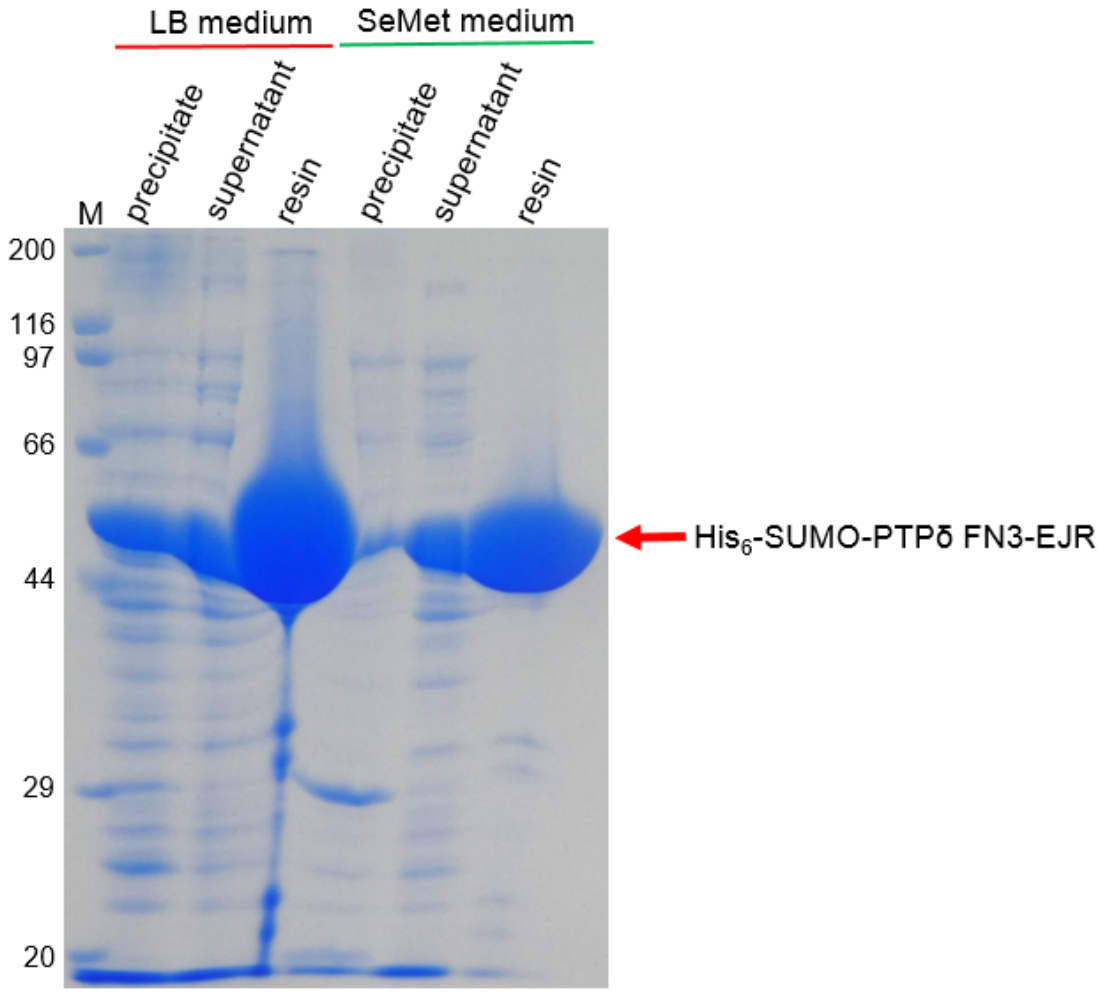

Figure 2-2 Expression check of mouse PTPδ FN3-EJR. The band of 'precipitant' represents insoluble fraction and the band of 'supernatant' represents soluble fraction of cell lysate. The band of 'resin' represents sample of Ni-NTA Superflow (QIAGEN) after washing by lysis buffer. The bands of His_6-SUMO-PTPδ FN3-EJR are indicated by red arrow.

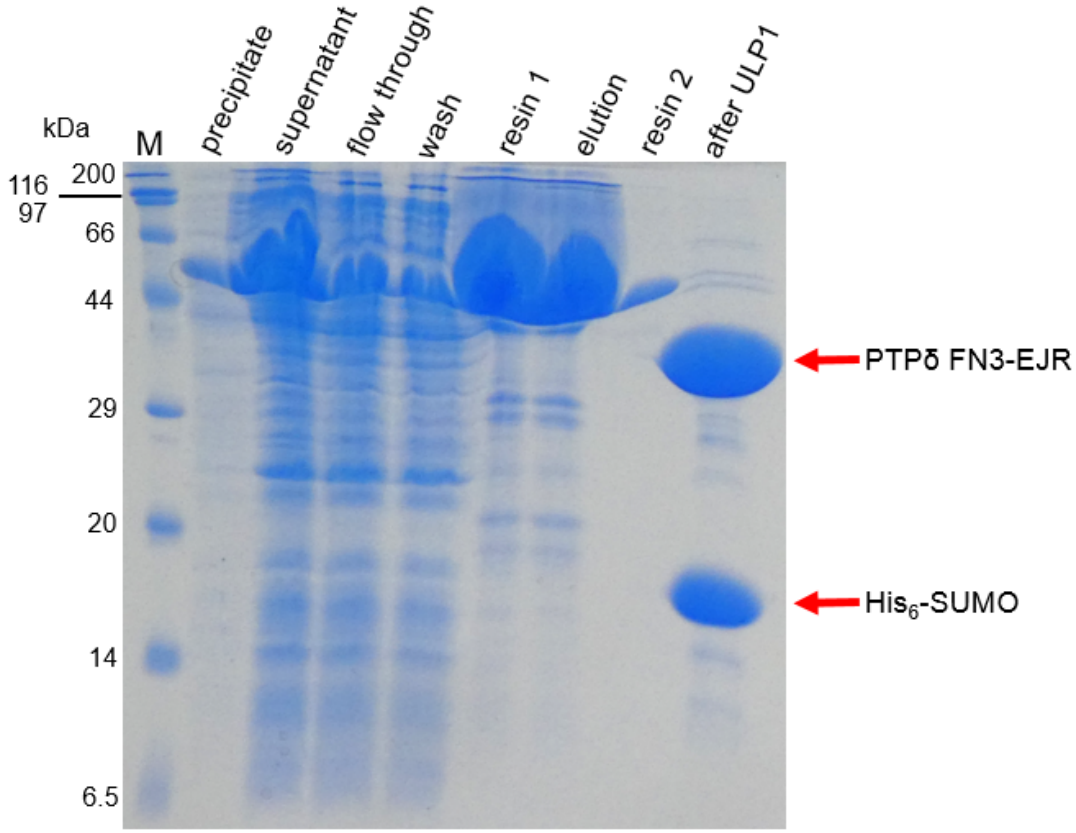

Figure 2-3 Purification of mouse PTPδ FN3-EJR by Ni-NTA affinity chromatography. The sample 'precipitant' represents insoluble fraction and the sample 'supernatant' represents soluble fraction of cell lysate. The sample 'resin 1' represents Ni-NTA resin after washing by wash buffer. The sample 'resin 2' represents Ni-NTA resin after elution. The sample 'after ULP1' represents the protein solution after overnight ULP1 cleavage. The bands of PTPδ FN3-EJR and His_6-SUMO are indicated by red arrow.

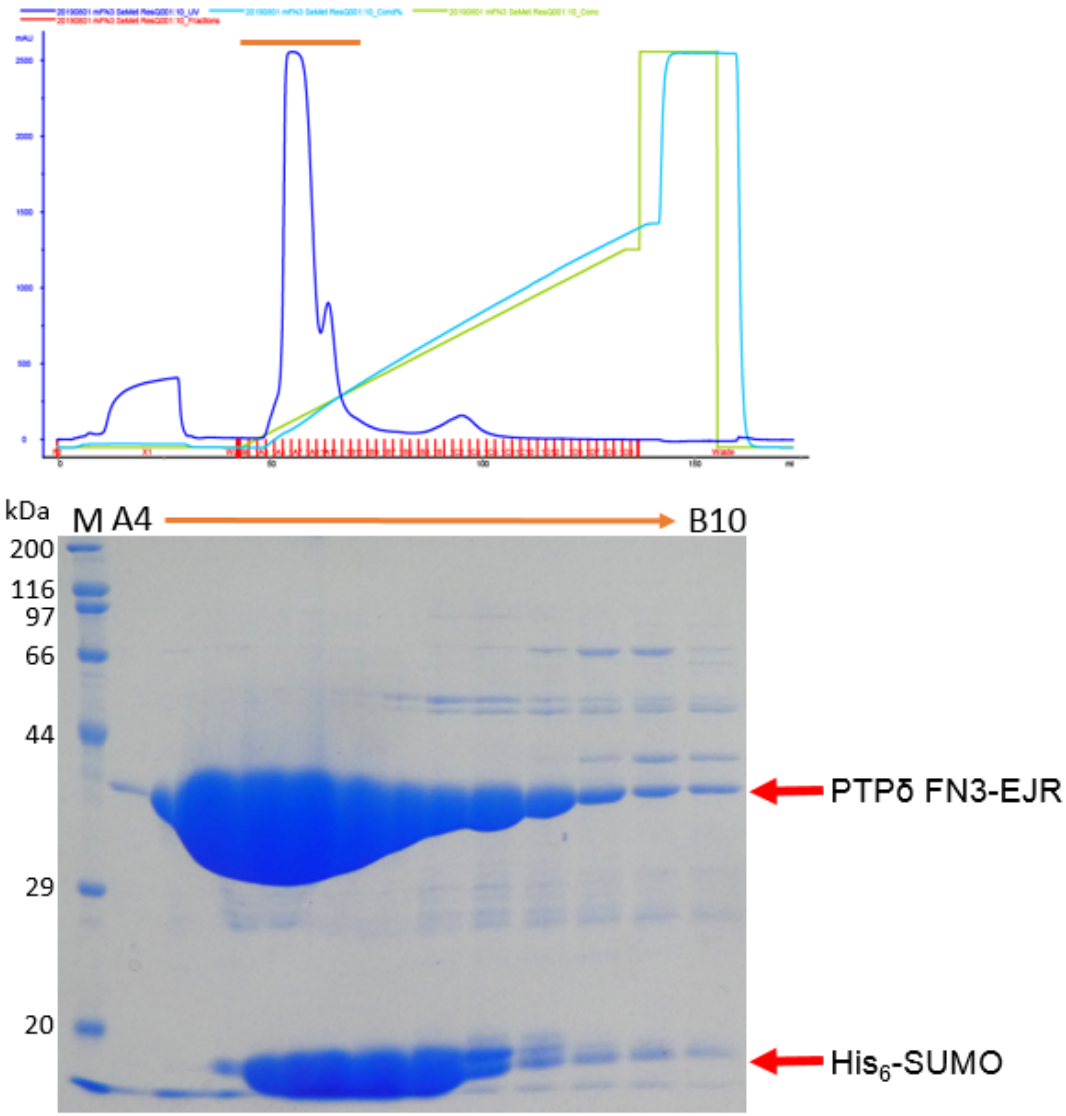

Figure 2-4 Purification of mouse PTPδ FN3-EJR by anion exchange chromatography. Fractions A4-B10 were collected for SDS-PAGE analysis. The bands of His_6-SUMO and PTPδ FN3-EJR are indicated by red arrow.

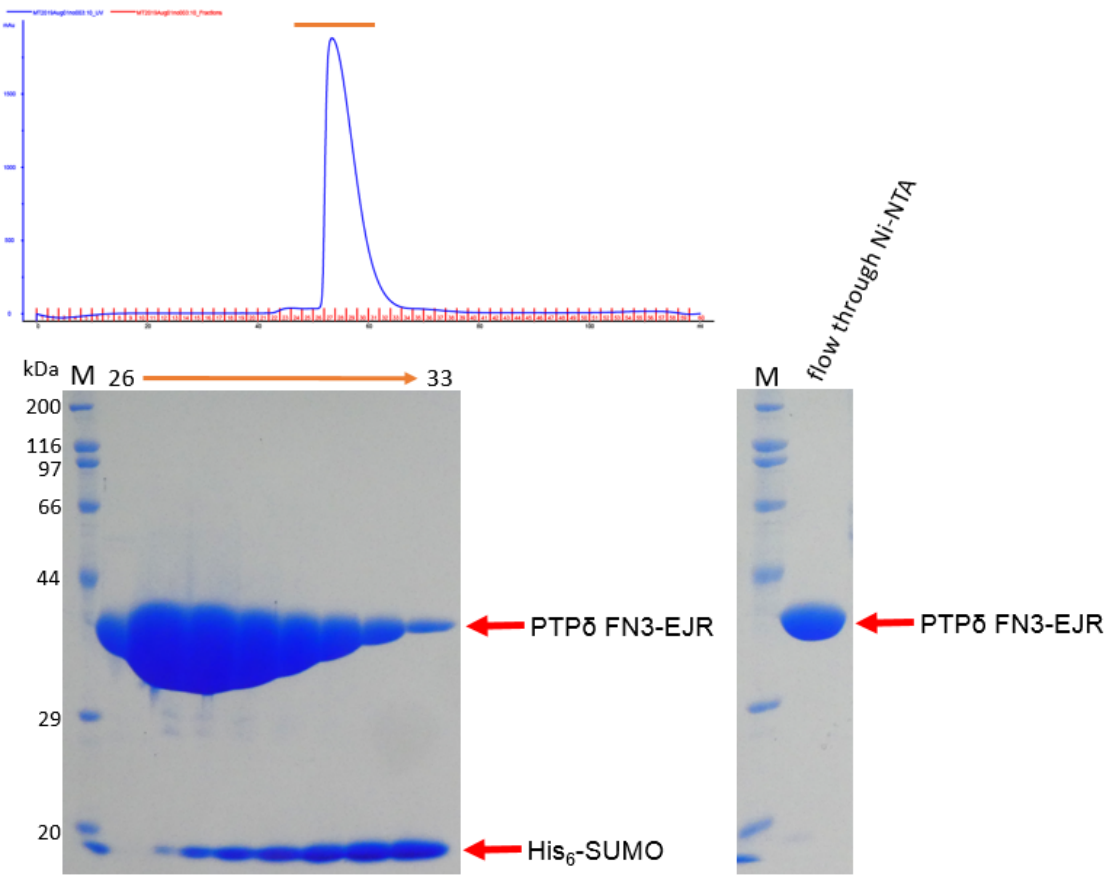

Figure 2-5 Purification of mouse PTPδ FN3-EJR by size exclusion chromatography and Ni-NTA affinity chromatography. Fractions 26-33 were collected for SDS-PAGE analysis. The protein sample was subjected to a Ni-NTA column to remove the remaining His_6-SUMO. The sample 'flow through Ni-NTA' indicates the protein solution after the second purification by Ni-NTA affinity chromatography. The bands of His_6-SUMO and PTPδ FN3-EJR are indicated by red arrow.

Chapter 3
Protein expression and purification of zebrafish PTPδ FN3-EJR

3.1 Introduction

In chapter 2, I described the expression system construction, the protein expression and purification processes of SeMet-labeled mouse PTPδ FN3-EJR. To deepen our understanding of the uncharacterized region of PTPδ extracellular domain, PTPδ FN3-EJR of other species could been studied. Here, I chose zebrafish PTPδ FN3-EJR as a study object.

Protein crystallizability is associated with surface properties and crystallization is driven by free energy change from the protein supersaturated solution to protein crystals in the solvent. Crystallization is quite sensitive to entropy changes in both the solvent and the protein. The Surface Entropy Reduction (SER) approach replaces the high-entropy amino acid residues such as lysines and glutamines with residues that have low-entropy side chains like alanines [34]. Mutants that are likely to enhance the protein crystallizability is predicted by SERp Server.

In this chapter, I constructed the protein expression system of wild type zebrafish PTPδ FN3-EJR and three mutants, using pET28aSUMO plasmid and *E.coli* strain. After the expression check, proteins were expressed in large-scale LB medium and purified with affinity chromatography, anion exchange chromatography and size exclusion chromatography. Finally, the highly purified zebrafish PTPδ FN3-EJR was concentrated for crystallization.

3.2 Materials and Methods

3.2.1 Expression system construction of zebrafish PTPδ FN3-EJR

The gene encoding zebrafish PTPδ FN3-EJR was synthesized by eurofins Genomics and used as the template for PCR. The PCR was performed with KOD One PCR Master Mix (TOYOBO). The reaction solution components and cycling conditions are shown in Figure 3-2. The DNA of zebrafish PTPδ FN3-EJR was assembled with linearized pET28aSUMO by Gibson Assembly.

The genes encoding the three mutants were also amplified by PCR. The DNA fragments of zebrafish PTPδ FN3-EJR mutants were assembled with linearized pET28aSUMO by Gibson Assembly, with the same experimental conditions as that of the wild type.

The four kinds of recombinant plasmids were mixed with competent cells respectively, and the mixtures were heat-shocked at 42°C for 45 s for transformation. Then 800 μL Lysogeny-Broth (LB) medium was added to each mixture and incubated at 37°C for 1h. Transformed *E.coli* cells were plated onto LB agar media containing kanamycin and incubated at 37°C overnight. Colony PCRs were performed, and the selected colonies were inoculated into four 5 mL LB medium containing kanamycin respectively and incubated at 37°C overnight. Plasmids were extracted and the inserted DNA fragments were confirmed by a DNA sequencing service (eurofins).

The verified recombinant plasmids were transformed into *E. coli* cells by electroporation, respectively. Then 800 μL LB medium was added to each mixture and the samples were incubated at 37°C for 1h. Transformed *E.coli* cells were plated onto LB agar media containing kanamycin respectively and incubated at 37°C overnight.

3.2.2 Expression check of zebrafish PTPδ FN3-EJR

For each of the wild type zebrafish PTPδ FN3-EJR and the three mutants, the expression check was performed as described below. Freshly transformed colonies were inoculated into 5 mL LB medium containing kanamycin and incubated at 37°C overnight. 200 μL *E.coli* suspension was transferred into 5 mL LB medium containing kanamycin and incubated at 37°C until OD_{600} reached 0.6. Protein expression was induced by adding IPTG. After incubation overnight, the cells were harvested by centrifugation at 5000 rpm for 10 min and resuspended in 1 mL lysis buffer. Buffers described in this chapter were the same as the buffers in chapter 2. Resuspended cells were lysed by sonication and centrifugated at 15000 rpm for 10 min at 4°C to remove cell debris. The supernatant was then applied to Ni-NTA Superflow resin (Qiagen) pre-equilibrated with lysis buffer and incubated at 4°C for 15 min. The supernatant fraction was removed after centrifugation at 700 × g for 5 min, then 200 μL lysis buffer was added to Ni-NTA resin for washing. After centrifugation at 700 × g for 5 min, the supernatant fraction was removed and the resin was sampled for SDS-PAGE analysis.

3.2.3 Large-scale expression and purification of zebrafish PTPδ FN3-EJR

For each of the wild type zebrafish PTPδ FN3-EJR and the three mutants, the large-scale expression and purification were performed as described below.

E.coli colonies were inoculated into 25 mL LB medium containing kanamycin and incubated at 37°C overnight. The 25 mL *E.coli* suspension was transferred into 2.5 L LB medium containing kanamycin and incubated at 37°C until OD_{600} reached almost 0.6. IPTG was added to induce protein expression. After incubation overnight, the cells were harvested by centrifugation at 7000 rpm for 10 min and resuspended in 100 mL lysis

buffer. Resuspended cells were lysed by sonication and centrifugated at 17000 rpm for 1h at 4°C.

The supernatant was applied to Ni-NTA Superflow resin pre-equilibrated with lysis buffer and incubated at 4°C for 15 min. The fraction of flow through was collected for sampling and the Ni-NTA column was washed with 50 mL wash buffer. His_6-SUMO-PTPδ was then eluted with 25 mL elution buffer. ULP1 was added to the protein elution with the ratio of 1:200 (w/w) to cleave down the His_6-SUMO tag. The elution was dialyzed against dialysis buffer at 4°C overnight to lower the concentration of NaCl.

Anion exchange chromatography was applied for protein purification with Resource Q 6 mL column (GE Healthcare), using buffer A and buffer B. The protein fractions were collected and concentrated to 500 μL with Vivaspin 20 (10000 MWCO PES) (Sartorius). The sample was then applied to a HiLoad 16/60 Superdex 75 column (GE Healthcare) for size exclusion chromatography. Protein purification processes were performed by AKTApurifier (GE Healthcare). The purified fractions were confirmed by SDS-PAGE and concentrated with Vivaspin 20 (10000 MWCO PES) (Sartorius). The absorbance of the protein at 280 nm was measured with Nanodrop ND2000 (Thermo Fisher). The concentration of the protein was calculated by the absorbance at 280 nm and the molar extinction coefficient. The concentrated protein sample was dispensed into several microtubes, flash frozen in liquid nitrogen and stored at -80°C.

3.3 Results and Discussion

3.3.1 Expression check of zebrafish PTPδ FN3-EJR

The recombinant zebrafish PTPδ FN3-EJR proteins, both the wild type and the three mutants, were expressed in *E. coli* cells and can be found in the soluble fraction after lysis (Figure 3-4). The band of His_6-SUMO-PTPδ can be detected in resin fraction on SDS-PAGE gel, indicates that his_6-SUMO-PTPδ bond to Ni-NTA resin successfully by the binding affinity of His_6 toward Ni-NTA. After the expression check, large-scale expressions in 2.5 L LB media were performed.

3.3.2 Large-scale expression and purification of zebrafish PTPδ FN3-EJR

The supernatant fractions containing His_6-SUMO-tagged zebrafish PTPδ FN3-EJR proteins were added to pre-equilibrated Ni-NTA columns respectively for affinity chromatography, and the results are shown in Figure 3-5 and Figure 3-6. The target proteins can be found in the soluble fractions after lysis, while there were still some target proteins existed in precipitate. His_6-SUMO-PTPδ FN3-EJRs bond to Ni-NTA resin and most of contaminant proteins were removed after washing. The target proteins were then eluted into the 'elution' fractions while a small amount of the proteins remained on the Ni-NTA columns. The concentration of each protein was calculated by the absorbance at 280 nm and its molar extinction coefficient. The concentration of His_6-SUMO-zebrafish PTPδ FN3-EJR (wild type) was 1.65g/L, the concentration of mutant-560 was 2.73 g/L, the concentration of mutant-576 was 1.15 g/L and the concentration of mutant-739 was 1.02 g/L. After the overnight digestion with ULP1, zebrafish PTPδ FN3-EJR proteins were successfully cleaved away from His_6-SUMO tags.

The mixtures of the target proteins and His_6-SUMO were further purified by anion-exchange chromatography and size exclusion chromatography to remove His_6-SUMO and obtain highly purified zebrafish PTPδ FN3-EJRs. The protein samples were subjected to a Resource Q 6 mL column (GE Healthcare) and all the four types of zebrafish PTPδ FN3-EJRs were eluted at a NaCl concentration of approximately 0.2 M. The eluted fractions were analyzed by SDS-PAGE. The results were shown in Figure 3-7, Figure 3-8 and Figure 3-9. There was only one sharp peak during the anion exchange chromatography of zebrafish PTPδ FN3-EJR wild type, but two protein bands appeared on SDS-PAGE gel, indicating that some impurities still existed after purification. The situations of zebrafish PTPδ FN3-EJR mutant-560 and mutant-576 were the same. As for zebrafish PTPδ FN3-EJR mutant-739, the situation was more complicated. Several peaks appeared during its anion exchange chromatography process, and all of them were analyzed by SDS-PAGE. It seems that all the fractions we analyzed contained our target protein, but different impurities were there in the fractions. Fractions were collected and concentrated respectively for further purifications by a HiLoad 16/60 Superdex 75 column (GE Healthcare).

The results of size exclusion chromatography and SDS-PAGE analysis were shown in Figure 3-10 and Figure 3-11. Zebrafish PTPδ FN3-EJR mutant-739 was highly purified and the impurities were almost completely removed by size exclusion chromatography. The highly purified zebrafish PTPδ FN3-EJR mutant-739 was concentrated to 300 μL, and the concentration of the protein was calculated to be 17.00 g/L. As for zebrafish PTPδ FN3-EJR wild type, mutant-560 and mutant-576, the upper bands still existed even after the purification by size exclusion chromatography. It is quite strange that the impurities could not be removed since their molecular weights were much larger than the target

proteins. Furthermore, by comparing the SDS-PAGE results of Ni-NTA affinity chromatography, anion exchange chromatography and size exclusion chromatography, I found that the impurities were increasing during the purification process. Zebrafish PTPδ FN3-EJR wild type were concentrated to 10.30 g/L, 800 μL; mutant-560 and mutant-576 were concentrated to 22.50 g/L, 600 μL and 28.40 g/L, 200 μL, respectively.

3.4 Summary

In this chapter, three mutants of zebrafish PTPδ FN3-EJR were made to enhance the protein crystallizability. The expression systems of wild type zebrafish PTPδ FN3-EJR and its three mutants were constructed for protein expression in *E.coli* cells. After confirming the expression level in small scale, these four kinds of proteins were expressed in large scale and purified by Ni-NTA affinity chromatography, followed by anion exchange chromatography and size exclusion chromatography. Finally, wild type zebrafish PTPδ FN3-EJR and its three mutants were all concentrated for crystallization.

Reaction solution:

Milli-Q water	4.7 μL
KOD One PCR Master Mix	5 μL
10 pmol/μL forward primer	0.1 μL
10 pmol/μL reverse primer	0.1 μL
template DNA	0.1 μL
Total reaction volume	10 μL

PCR cycling conditions:

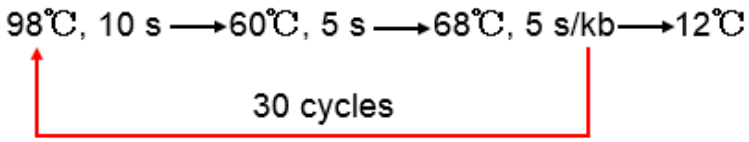

Figure 3-2 PCR reaction solution components and cycling conditions of zebrafish PTPδ FN3-EJR.

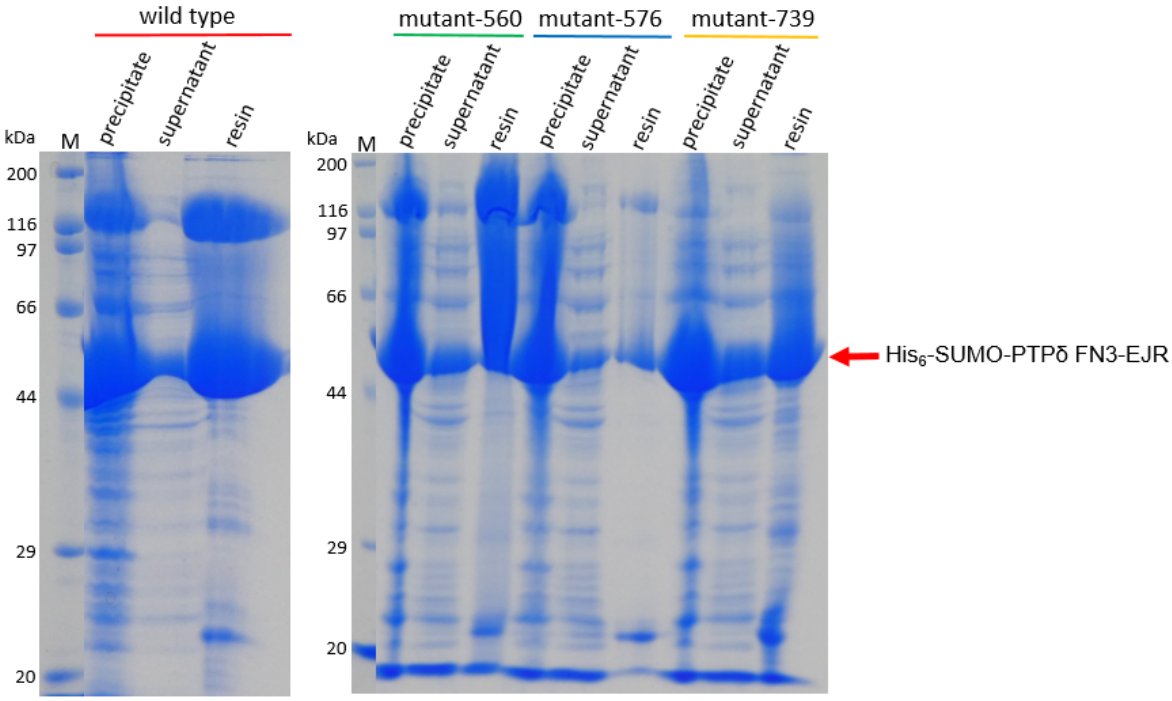

Figure 3-4 Expression check of zebrafish PTPδ FN3-EJR wild type and its three mutants. The band of 'precipitant' represents insoluble fraction and the band of 'supernatant' represents soluble fraction of cell lysate. The band of 'resin' represents sample of Ni-NTA Superflow (QIAGEN) after washing by lysis buffer. The bands of His_6-SUMO-PTPδ FN3-EJR are indicated by red arrow.

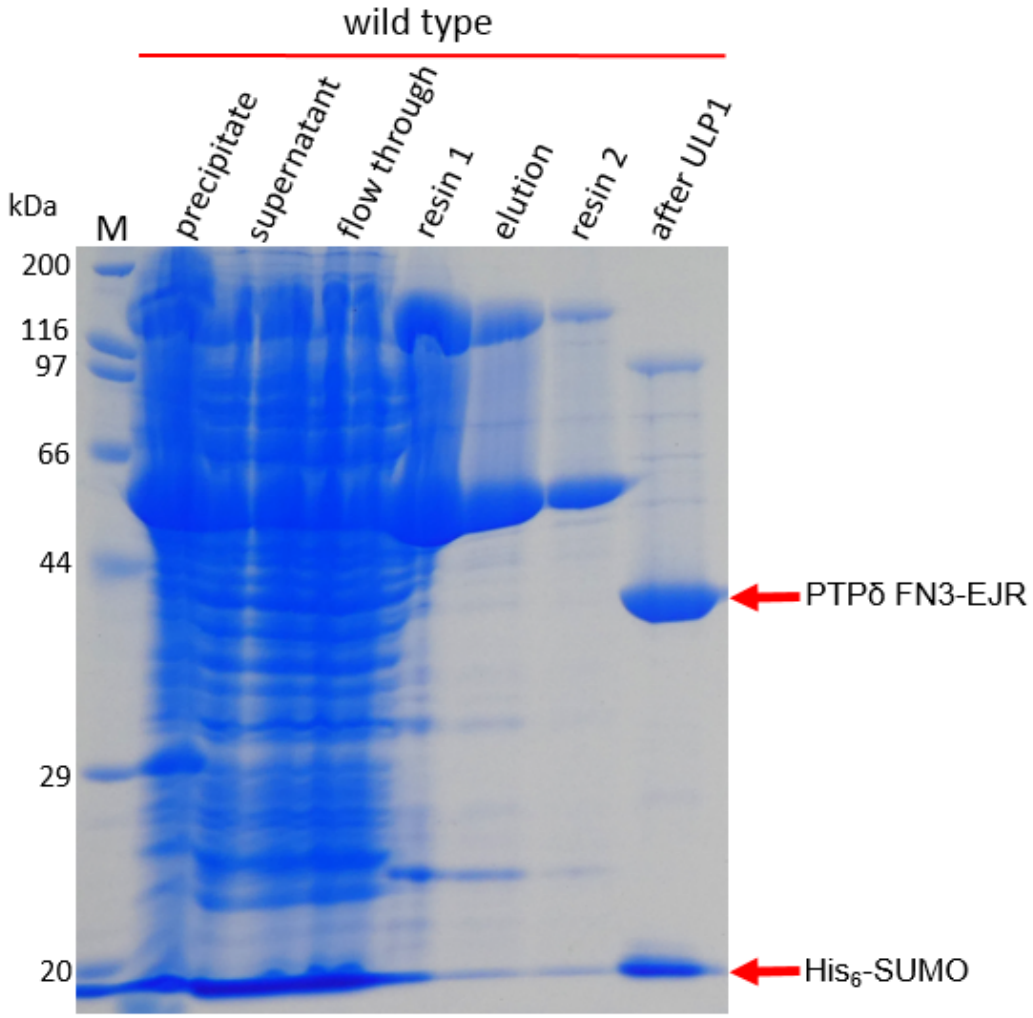

Figure 3-5 Purification of zebrafish PTPδ FN3-EJR wild type by Ni-NTA affinity chromatography. The sample 'precipitant' represents insoluble fraction and the sample 'supernatant' represents soluble fraction of cell lysate. The sample 'resin 1' represents Ni-NTA resin after washing by wash buffer. The sample 'resin 2' represents Ni-NTA resin after elution. The sample 'after ULP1' represents the protein solution after overnight ULP1 cleavage. The bands of PTPδ FN3-EJR and His_6-SUMO are indicated by red arrow.

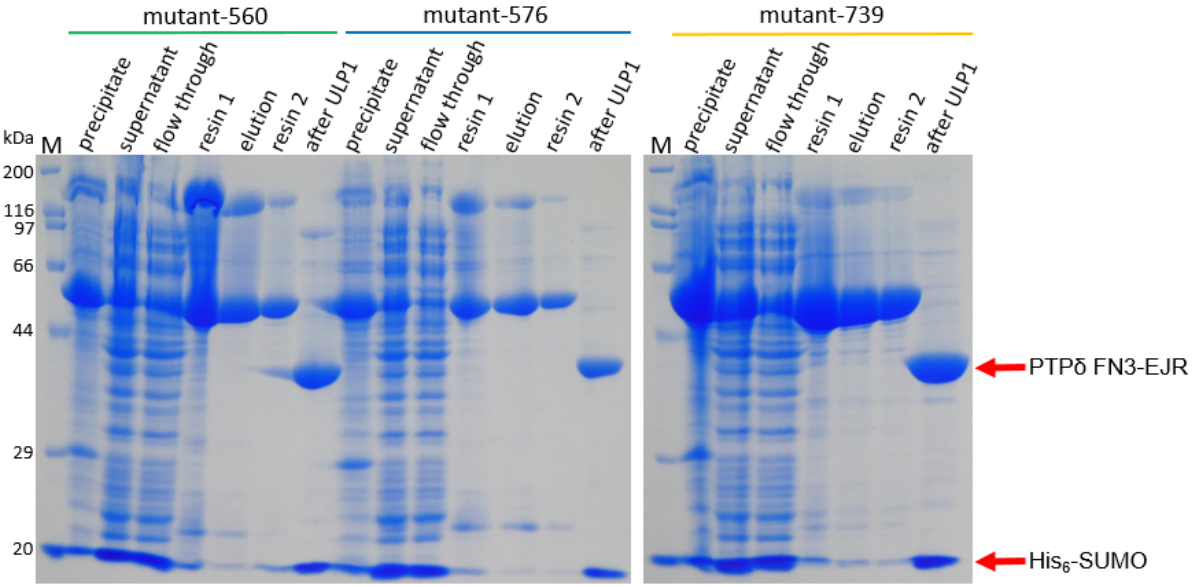

Figure 3-6 Purification of zebrafish PTPδ FN3-EJR mutants by Ni-NTA affinity chromatography. The sample 'precipitant' represents insoluble fraction and the sample 'supernatant' represents soluble fraction of cell lysate. The sample 'resin 1' represents Ni-NTA resin after washing by wash buffer. The sample 'resin 2' represents Ni-NTA resin after elution. The sample 'after ULP1' represents the protein solution after overnight ULP1 cleavage. The bands of PTPδ FN3-EJR and His_6-SUMO are indicated by red arrow.

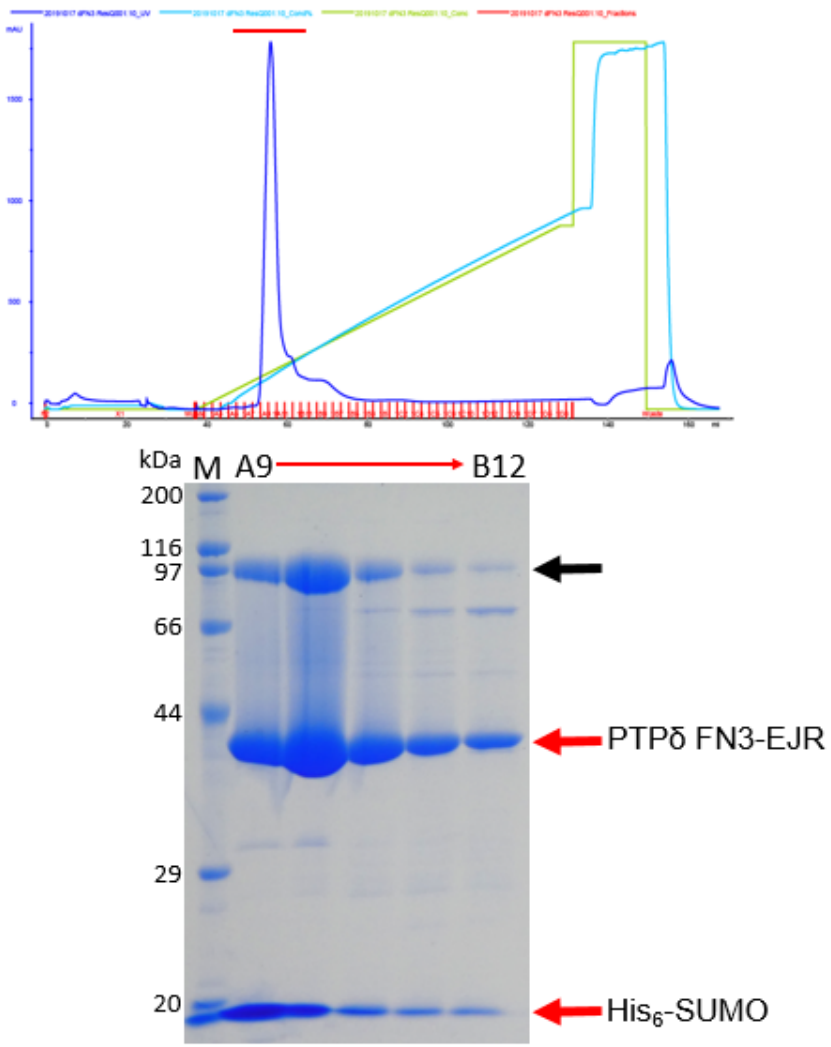

Figure 3-7 Purification of zebrafish PTPδ FN3-EJR wild type by anion exchange chromatography. Fractions A9-B12 were collected for SDS-PAGE analysis. The bands of His_6-SUMO and PTPδ FN3-EJR are indicated by red arrow. The upper band of the impurity is indicated by black arrow.

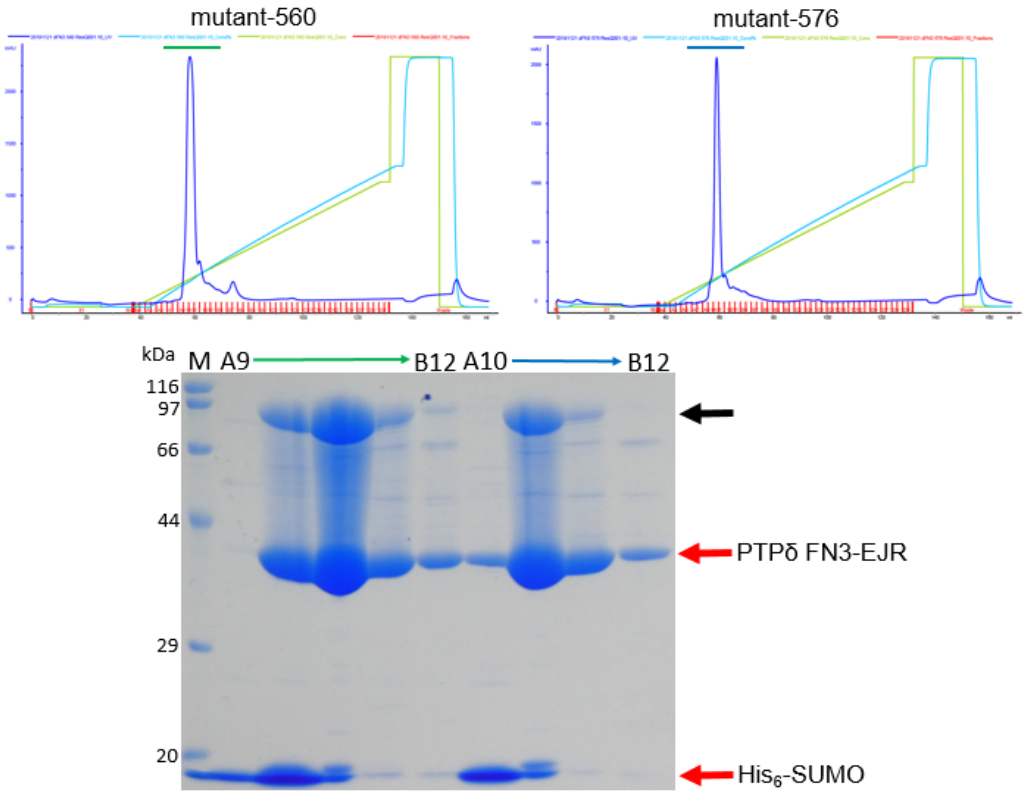

Figure 3-8 Purifications of zebrafish PTPδ FN3-EJR mutant-560 and mutant-576 by anion exchange chromatography. Fractions A9-B12 of mutant-560 and A10-B12 of mutant-576 were collected for SDS-PAGE analysis. The bands of His_6-SUMO and PTPδ FN3-EJR are indicated by red arrow. The upper bands of the impurities are indicated by black arrow.

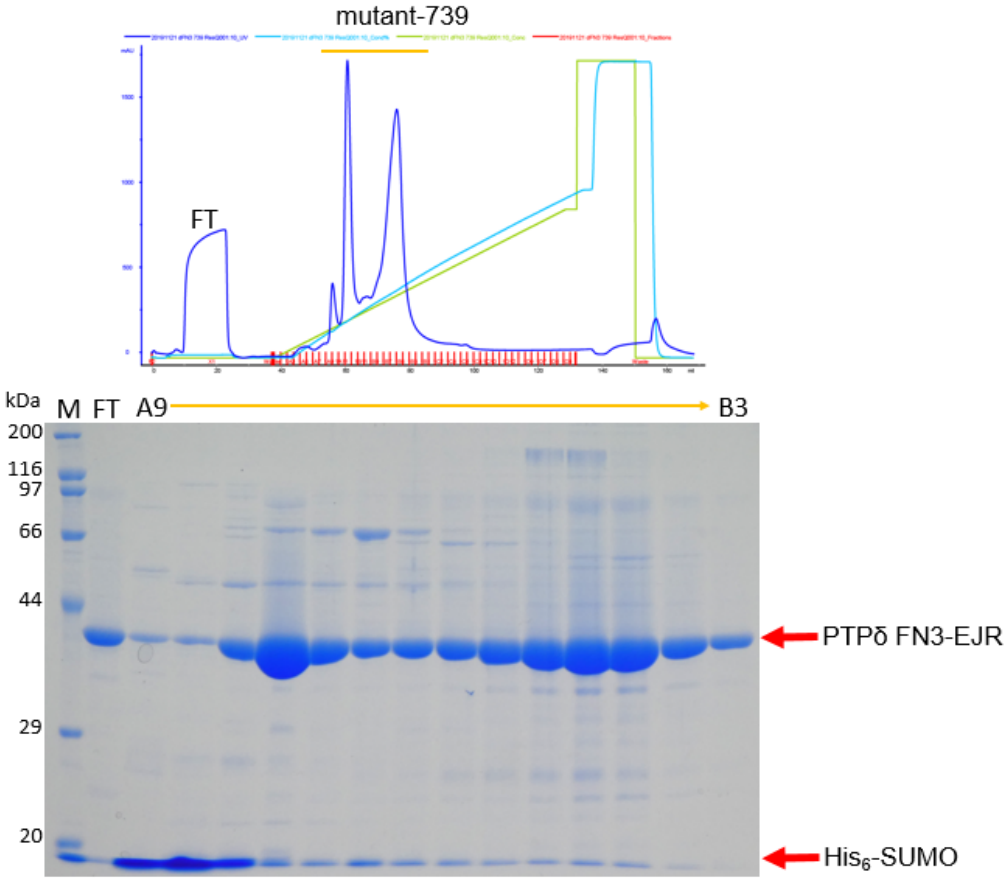

Figure 3-9 Purification of zebrafish PTPδ FN3-EJR mutant-739 by anion exchange chromatography. Fractions A9-B3 were collected for SDS-PAGE analysis. The bands of His_6-SUMO and PTPδ FN3-EJR are indicated by red arrow.

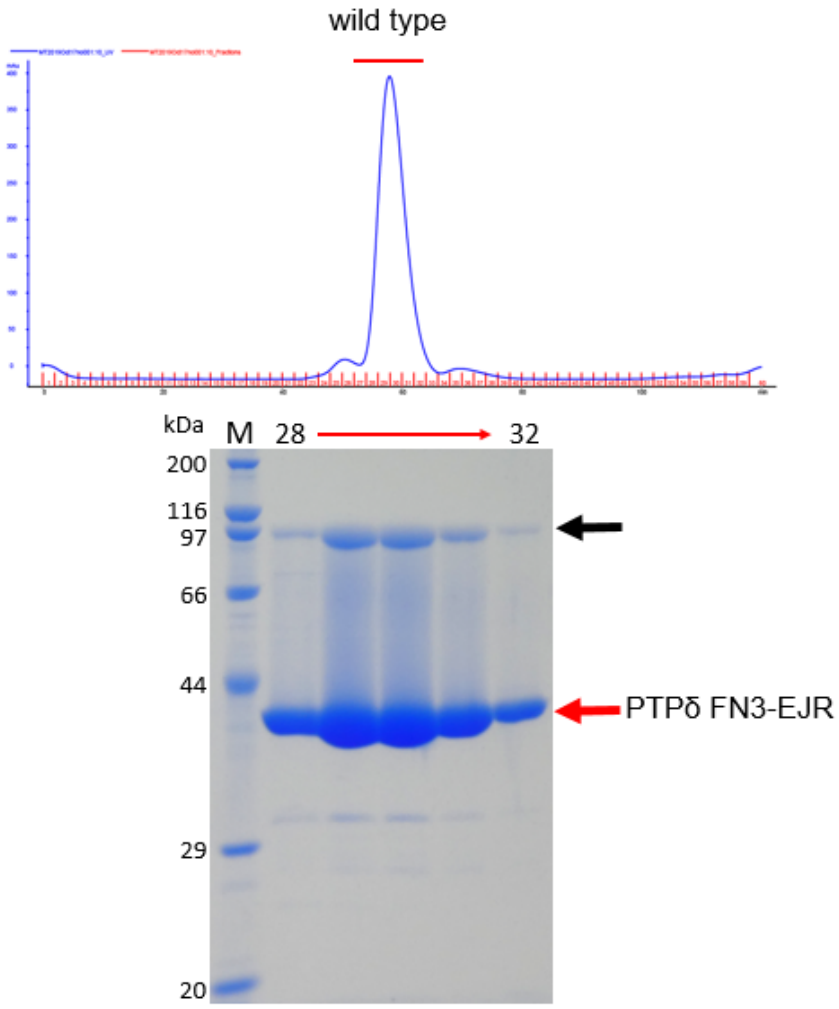

Figure 3-10 Purification of zebrafish PTPδ FN3-EJR wild type by size exclusion chromatography. Fractions 28-32 were collected for SDS-PAGE analysis. Wild type zebrafish PTPδ FN3-EJR is indicated by red arrow. The impurity is indicated by black arrow.

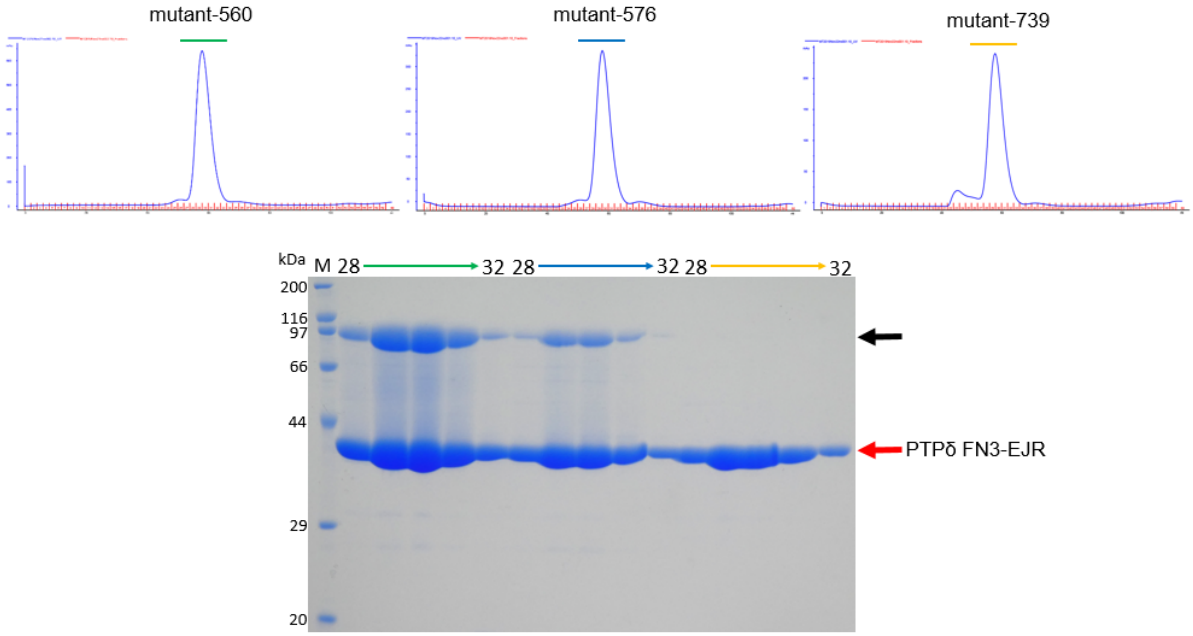

Figure 3-11 Purifications of zebrafish PTPδ FN3-EJR mutant-560, mutant-576 and mutant-739 by size exclusion chromatography. Fractions 28-32 of each protein were collected for SDS-PAGE analysis. Zebrafish PTPδ FN3-EJR is indicated by red arrow and the impurities are indicated by black arrow.

Chapter 4
Crystallization of mouse PTPδ FN3-EJR and zebrafish PTPδ FN3-EJR

4.1 Introduction

The functions of biological macromolecules can be inferred by their three-dimensional structure [35]. X-ray crystallography is an extensively applied tool of structural biology, which plays a significant role in uncovering the secrets of life [36]. Until 2011, over 80% of the Protein Data Bank entries are protein structures that were determined by X-ray crystallography. The macromolecules such as proteins must be purified to homogeneity, or at least as close as possible to homogeneity, to obtain crystals which are suitable for crystallographic studies. The sitting drop vapor diffusion method is a popular technique for crystallization of protein [37] (Figure 4-1). The drop composed of reagent and protein sample is placed in a vapor equilibration with the reservoir of reagent. Typically the drop always contains lower concentration of reagent than the reservoir. The relative supersaturation of the protein increases as water leaves the drop and gradually the protein solution develops into crystals.

In this chapter, I described the processes of initial screenings and crystal refinements of both mouse PTPδ FN3-EJR and zebrafish PTPδ FN3-EJR. After several steps of crystal refinements, crystals suitable for crystallographic studies were obtained and used for subsequent X-ray diffraction experiments.

4.2 Materials and Methods

4.2.1 Crystallization of mouse PTPδ FN3-EJR

Highly purified SeMet-labeled mouse PTPδ FN3-EJR was adjusted to 10 g/L with SEC buffer and prepared for sitting drop vapor diffusion method. Standard crystal screening kits (Hampton Research) were used for initial crystal screening of SeMet-labeled mouse PTPδ FN3-EJR. 200 nL protein sample was mixed with 200 nL reservoir solution and the mixtures were set on MRC 2 Well Crystallization plates (SWISSCI) by Mosquito liquid-handling robot (TTP Labtech). Crystallization plates were kept and checked regularly. When the initial crystals came out, several refinements were applied to improve the quality of the crystals. The mixtures of protein sample and precipitant solution were set on 24 well Cryschem M plates (Hampton Research) by hand and the plates were incubated.

4.2.2 Crystallization of zebrafish PTPδ FN3-EJR

Highly purified zebrafish PTPδ FN3-EJR proteins, both wild type and the three mutants, were adjusted to 10 g/L with SEC buffer and prepared for sitting drop vapor diffusion method. Standard crystal screening kits (Hampton Research) were used for initial crystal screening of zebrafish PTPδ FN3-EJR proteins. The mixtures of 200 nL protein sample and 200 nL reservoir solution were set on MRC 2 Well Crystallization plates (SWISSCI) by Mosquito liquid-handling robot (TTP Labtech). Crystallization plates were kept and checked regularly. When the initial crystals came out, several refinements were applied to improve the quality of the crystals. The mixtures of protein sample and precipitant solution were set on 24 well Cryschem M plates (Hampton Research) by hand and the plates were incubated.

4.3 Results and Discussion

4.3.1 Crystallization of mouse PTPδ FN3-EJR

Crystals of mouse PTPδ FN3-EJR were found in initial screening plate. The crystallization conditions were adjusted for refinement. After the incubation for more than two weeks, crystals appeared. Further refinement has been done and we tried to improve the crystals. After several days, crystals appeared in wells. The qualities of crystals were improved a lot after refinements. Elaborate refinements were then performed. Finally, crystals with good qualities were obtained for diffraction data collection.

4.3.2 Crystallization of zebrafish PTPδ FN3-EJR

Crystals of zebrafish PTPδ FN3-EJR were found in initial screening plates. The refinements for crystallization have been done. After one day, crystals of zebrafish PTPδ FN3-EJR appeared and the quality of crystals were improved a lot after the refinement. Further refinement was performed to improve the crystals. Finally, zebrafish PTPδ FN3-EJR crystals with good qualities were obtained for diffraction data collection.

4.4 Summary

In this chapter, I described the crystallization processes of SeMet-labeled mouse PTPδ FN3-EJR and zebrafish PTPδ FN3-EJR. After several steps of crystallization refinement, high-quality single crystals were obtained for subsequent diffraction data collection.

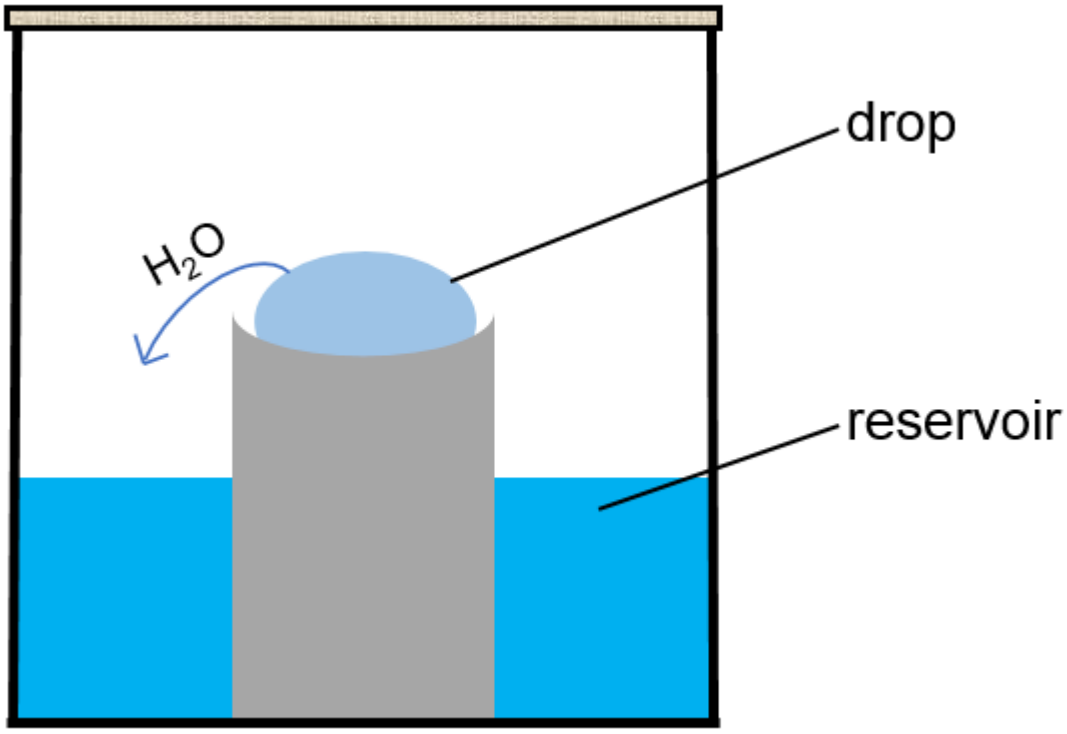

Figure 4-1 Sitting drop vapor diffusion method. The "drop" contains equal volume of our protein sample and reservoir solution (or drop solution) in subsequent figures. The relative supersaturation of the protein increases as water leaves the drop and gradually the protein solution develops into crystals.

Chapter 5
Structure determination and analysis of mouse PTPδ FN3-EJR and zebrafish PTPδ FN3-EJR

Chapter 5 cannot be disclosed because this part will be published in academic journal within five years.

Chapter 6
General discussion

6.1 Summary of this study

Type IIa RPTPs are among the most-characterized synaptic CAMs. They are originally linked to axon guidance and are recently highlighted as synaptic organizers. Type IIa RPTPs can induce synaptic differentiation by interacting with various postsynaptic adhesion molecules. Although the structural mechanism of the interaction between type IIa RPTPs and their postsynaptic ligands has been extensively studied by crystallography and other biophysical techniques, it remains unclear how the extracellular interaction transmits the signal into the intracellular domain, partly due to the lack of the structural information of the EJR domain of type IIa RPTPs.

In this study, I isolated a region including the EJR from mouse or zebrafish PTPδ, and investigated the structural feature of the extracellular domain of PTPδ near the cell membrane. In chapter 2, the expression system of mouse PTPδ FN3-EJR was constructed for protein expression in *E.coli* cells. After confirming the expression level in small scale, SeMet-labeled mouse PTPδ FN3-EJR was expressed and purified for crystallization. In chapter 3, three mutants of zebrafish PTPδ FN3-EJR were made to enhance the protein crystallizability. The expression systems of wild type zebrafish PTPδ FN3-EJR and its three mutants were constructed for protein expression in *E.coli* cells. These four kinds of proteins were expressed in large scale and purified for crystallization. In chapter 4, I described the crystallization processes of SeMet-labeled mouse PTPδ FN3-EJR and zebrafish PTPδ FN3-EJR. After several steps of crystallization refinement, high-quality single crystals were obtained for subsequent diffraction data collection. In chapter 5, I described the structure determination of SeMet-labeled mouse PTPδ FN3-EJR and zebrafish PTPδ FN3-EJR. This study provides the first atomic details of the EJR domain in type IIa RPTPs and provides the structural basis for the further functional study of this

extracellular juxtamembrane region.

6.2-6.6 cannot be disclosed because these parts will be published in academic journal within five years.

References

[1] Yamagata, A., Yoshida, T., Sato, Y., Goto-Ito, S., Uemura, T., Maeda, A., ... & Fukai, S. (2015). Mechanisms of splicing-dependent trans-synaptic adhesion by PTPδ–IL1RAPL1/IL-1RAcP for synaptic differentiation. Nature Communications, 6(1), 1-11.

[2] Batool, S., Raza, H., Zaidi, J., Riaz, S., Hasan, S., & Syed, N. I. (2019). Synapse formation: from cellular and molecular mechanisms to neurodevelopmental and neurodegenerative disorders. Journal of neurophysiology, 121(4), 1381-1397.

[3] Horstkorte, R., & Fuss, B. (2012). Cell adhesion molecules. In Basic Neurochemistry (pp. 165-179). Academic Press.

[4] Südhof, T. C. (2018). Towards an understanding of synapse formation. Neuron, 100(2), 276-293.

[5] Clandinin, T. R., Lee, C. H., Herman, T., Lee, R. C., Yang, A. Y., Ovasapyan, S., & Zipursky, S. L. (2001). Drosophila LAR regulates R1-R6 and R7 target specificity in the visual system. Neuron, 32(2), 237-248.

[6] Chagnon, M. J., Uetani, N., & Tremblay, M. L. (2004). Functional significance of the LAR receptor protein tyrosine phosphatase family in development and diseases. Biochemistry and cell biology, 82(6), 664-675.

[7] Tian, S. S., Tsoulfas, P., & Zinn, K. (1991). Three receptor-linked protein-tyrosine phosphatases are selectively expressed on central nervous system axons in the Drosophila embryo. Cell, 67(4), 675-685.

[8] Gershon, T. R., Baker, M. W., Nitabach, M., Wu, P., & Macagno, E. R. (1998). Two receptor tyrosine phosphatases of the LAR family are expressed in the developing leech by specific central neurons as well as select peripheral neurons, muscles, and other cells.

Journal of Neuroscience, 18(8), 2991-3002.

[9] Streuli, M., Krueger, N. X., Ariniello, P. D., Tang, M., Munro, J. M., Blattler, W. A., ... & Saito, H. (1992). Expression of the receptor‐linked protein tyrosine phosphatase LAR: proteolytic cleavage and shedding of the CAM‐like extracellular region. The EMBO Journal, 11(3), 897-907.

[10] Yan, H., Grossman, A., Wang, H. O. N. G., D'Eustachio, P., Mossie, K., Musacchio, J. M., ... & Schlessinger, J. (1993). A novel receptor tyrosine phosphatase-sigma that is highly expressed in the nervous system. Journal of Biological Chemistry, 268(33), 24880-24886.

[11] Coles, C. H., Jones, E. Y., & Aricescu, A. R. (2015, January). Extracellular regulation of type IIa receptor protein tyrosine phosphatases: mechanistic insights from structural analyses. In Seminars in cell & developmental biology (Vol. 37, pp. 98-107). Academic Press.

[12] Goto-Ito, S., Yamagata, A., Sato, Y., Uemura, T., Shiroshima, T., Maeda, A., ... & Fukai, S. (2018). Structural basis of trans-synaptic interactions between PTPδ and SALMs for inducing synapse formation. Nature communications, 9(1), 1-9.

[13] Takahashi, H., Arstikaitis, P., Prasad, T., Bartlett, T. E., Wang, Y. T., Murphy, T. H., & Craig, A. M. (2011). Postsynaptic TrkC and presynaptic PTPσ function as a bidirectional excitatory synaptic organizing complex. Neuron, 69(2), 287-303.

[14] Yoshida, T., Shiroshima, T., Lee, S. J., Yasumura, M., Uemura, T., Chen, X., ... & Mishina, M. (2012). Interleukin-1 receptor accessory protein organizes neuronal synaptogenesis as a cell adhesion molecule. Journal of Neuroscience, 32(8), 2588-2600.

[15] Won, S. Y., & Kim, H. M. . (2018). Structural basis for LAR-RPTP-mediated synaptogenesis. Moleculer Cells, 41(7).

[16] Takahashi, H., & Craig, A. M. (2013). Protein tyrosine phosphatases PTPδ, PTPσ, and LAR: presynaptic hubs for synapse organization. Trends in neurosciences, 36(9), 522-534.

[17] Um, J. W., & Ko, J. (2013). LAR-RPTPs: synaptic adhesion molecules that shape synapse development. Trends in cell biology, 23(10), 465-475.

[18] Pinto, D., Pagnamenta, A. T., Klei, L., Anney, R., Merico, D., Regan, R., ... & Almeida, J. (2010). Functional impact of global rare copy number variation in autism spectrum disorders. Nature, 466(7304), 368-372.

[19] Malhotra, D., McCarthy, S., Michaelson, J. J., Vacic, V., Burdick, K. E., Yoon, S., ... & Gill, M. (2011). High frequencies of de novo CNVs in bipolar disorder and schizophrenia. Neuron, 72(6), 951-963.

[20] Deng, W., & Li, R. (2015). Juxtamembrane contribution to transmembrane signaling. Peptide Science, 104(4), 317-322.

[21] Brooks, A. J., Dai, W., O'Mara, M. L., Abankwa, D., Chhabra, Y., Pelekanos, R. A., ... & Parker, M. W. (2014). Mechanism of activation of protein kinase JAK2 by the growth hormone receptor. Science, 344(6185).

[22] Erickson-Miller, C. L., DeLorme, E., Tian, S. S., Hopson, C. B., Stark, K., Giampa, L., ... & Miller, S. G. (2005). Discovery and characterization of a selective, nonpeptidyl thrombopoietin receptor agonist. Experimental hematology, 33(1), 85-93.

[23] Kim, M. J., Park, S. H., Opella, S. J., Marsilje, T. H., Michellys, P. Y., Seidel, H. M., & Tian, S. S. (2007). NMR structural studies of interactions of a small, nonpeptidyl Tpo mimic with the thrombopoietin receptor extracellular juxtamembrane and transmembrane domains. Journal of Biological Chemistry, 282(19), 14253-14261.

[24] Matthews, E. E., Thévenin, D., Rogers, J. M., Gotow, L., Lira, P. D., Reiter, L. A., ...

& Engelman, D. M. (2011). Thrombopoietin receptor activation: transmembrane helix dimerization, rotation, and allosteric modulation. The FASEB Journal, 25(7), 2234-2244.

[25] Kaplan, D. R., Hempstead, B. L., Martin-Zanca, D., Chao, M. V., & Parada, L. F. (1991). The trk proto-oncogene product: a signal transducing receptor for nerve growth factor. Science, 252(5005), 554-558.

[26] Shen, J., Sun, D., Shao, J., Chen, Y., Pang, K., Guo, W., & Lu, B. (2019). Extracellular juxtamembrane motif critical for TrkB preformed dimer and activation. Cells, 8(8), 932.

[27] Su, P. C., & Berger, B. W. (2012). Identifying key juxtamembrane interactions in cell membranes using AraC-based transcriptional reporter assay (AraTM). Journal of Biological Chemistry, 287(37), 31515-31526.

[28] Deng, W., Cho, S., Su, P. C., Berger, B. W., & Li, R. (2014). Membrane-enabled dimerization of the intrinsically disordered cytoplasmic domain of ADAM10. Proceedings of the National Academy of Sciences, 111(45), 15987-15992.

[29] EL Craig, S., & M Brady-Kalnay, S. (2011). Tumor-derived extracellular fragments of receptor protein tyrosine phosphatases (RPTPs) as cancer molecular diagnostic tools. Anti-Cancer Agents in Medicinal Chemistry (Formerly Current Medicinal Chemistry-Anti-Cancer Agents), 11(1), 133-140.

[30] Streuli, M., Krueger, N. X., Ariniello, P. D., Tang, M., Munro, J. M., Blattler, W. A., ... & Saito, H. (1992). Expression of the receptor‐linked protein tyrosine phosphatase LAR: proteolytic cleavage and shedding of the CAM‐like extracellular region. The EMBO Journal, 11(3), 897-907.

[31] Bellizzi, J. J., Widom, J., Kemp, C. W., & Clardy, J. (1999). Producing selenomethionine-labeled proteins with a baculovirus expression vector system. Structure,

7(11), R263-R267.

[32] Wenzel, S., Imasaki, T., & Takagi, Y. (2019). A practical method for efficient and optimal production of Seleno-methionine-labeled recombinant protein complexes in the insect cells. Protein science : a publication of the Protein Society, 28(4), 808–822.

[33] Leahy, D. J., Hendrickson, W. A., Aukhil, I., & Erickson, H. P. (1992). Structure of a fibronectin type III domain from tenascin phased by MAD analysis of the selenomethionyl protein. Science, 258(5084), 987-991.

[34] Derewenda, Z. S. (2004). Rational protein crystallization by mutational surface engineering. Structure, 12(4), 529-535.

[35] Dessau, M. A., & Modis, Y. (2011). Protein crystallization for X-ray crystallography. JoVE (Journal of Visualized Experiments), (47), e2285.

[36] Shi, Y. (2014). A glimpse of structural biology through X-ray crystallography. Cell, 159(5), 995-1014.

[37] McPherson, A. (2004). Introduction to protein crystallization. Methods, 34(3), 254-265.

[38] Liu, Q., & Hendrickson, W. A. (2017). Contemporary use of anomalous diffraction in biomolecular structure analysis. In Protein Crystallography (pp. 377-399). Humana Press, New York, NY.

[39] Hunter, M. S., Yoon, C. H., DeMirci, H., Sierra, R. G., Dao, E. H., Ahmadi, R., ... & Hayes, M. J. (2016). Selenium single-wavelength anomalous diffraction de novo phasing using an X-ray-free electron laser. Nature communications, 7(1), 1-5.

[40] Lebedev, A. A., Vagin, A. A., & Murshudov, G. N. (2008). Model preparation in MOLREP and examples of model improvement using X-ray data. Acta Crystallographica Section D: Biological Crystallography, 64(1), 33-39.

[41] Minor, W., & Otwinowski, Z. (1997). Processing of X-ray diffraction data collected in oscillation mode. Methods Enzymol, 276(307.10), 1016.

[42] Winn, M. D., Ballard, C. C., Cowtan, K. D., Dodson, E. J., Emsley, P., Evans, P. R., ... & McNicholas, S. J. (2011). Overview of the CCP4 suite and current developments. Acta Crystallographica Section D: Biological Crystallography, 67(4), 235-242.

[43] Emsley, P., Lohkamp, B., Scott, W. G., & Cowtan, K. (2010). Features and development of Coot. Acta Crystallographica Section D: Biological Crystallography, 66(4), 486-501.

[44] Adams, P. D., Afonine, P. V., Bunkóczi, G., Chen, V. B., Davis, I. W., Echols, N., ... & McCoy, A. J. (2010). PHENIX: a comprehensive Python-based system for macromolecular structure solution. Acta Crystallographica Section D: Biological Crystallography, 66(2), 213-221.

[45] Yuan, S., Chan, H. S., Filipek, S., & Vogel, H. (2016). PyMOL and Inkscape bridge the data and the data visualization. Structure, 24(12), 2041-2042.

[46] Jaaks, P., & Bernasconi, M. (2017). The proprotein convertase furin in tumour progression. International Journal of Cancer, 141(4), 654-663.

Acknowledgements

I am deeply indebted to my supervisor, Prof. Shuya Fukai whose supervision and encouragement were indispensable for my PhD study. I received so many helpful comments and advice not only with regard to my research but also on how to be a good researcher.

My sincere thanks also goes to Dr. Yusuke Sato and Dr. Kei Okatsu who have helped me a lot with my experiments and structural analysis.

Moreover, I sincerely thank Prof. Yukihide Tomari, Dr. Atsushi Yamagata, Dr. Sakurako Goto-Ito, and techinicians Dr. Tomoko Shiroshima, Miss. Asami Maeda. Without their precious support, it would not be possible to conduct this research.

I would like to thank the staffs at SPring-8 for their kind help and technical support during data collection

Last but not the least, I would like to thank my family, especially my mother Mrs. Shuying Song, for their continuous support and encouragement throughout the doctoral course and my life in general.